Humidity Impact on Streamer Inception Parameters for Turn-to-Turn Insulation of Inverter-Fed Motors

Hadi Naderiallaf[1], Yatai Ji[2], Paolo Giangrande[3], Michael Galea[4], Michele Degano[1], Christopher Gerada[1]

[1]*Power Electronics, Machine and Control Group (PEMC), University of Nottingham, Nottingham,* The United Kingdom

[2]*Key Laboratory of More Electric Aircraft Technology of Zhejiang Province, University of Nottingham Ningbo,* Ningbo, China

[3]*Department of Engineering and Applied Sciences, University of Bergamo,* Dalmine, Italy

[4]*Department of Industrial Electrical Power Conversion, University of Malta,* Msida, Malta

Hadi.Naderiallaf@nottingham.ac.uk

Abstract- **This study explores the impact of varying relative humidity (RH) levels (30%-90%) at 90°C on streamer inception parameters (SIPs) compared to those at 25°C. Schumann's streamer inception criterion (SCSIC) is used to assess the vulnerability of turn-to-turn insulation in inverter-fed motors with rising humidity at 90°C. The analysis includes SIPs such as effective ionization coefficient of air (α_{eff}), partial discharge (PD) inception field (E_{inc}), critical field line length (CFLL), and firing voltage (V_{firing}). Furthermore, this study emphasizes the humidity-dependent shift in the Schumann constant (i.e., the natural logarithm of the critical electron number that determines the Townsend-to-streamer discharge transition, K) from 25°C to 90°C and advises caution when using the derived K at room temperature (e.g., 25°C) to predict PDIV at higher temperatures (e.g., 90°C), especially when RH≥50%.**

I. INTRODUCTION

In inverter-fed motors, turn-to-turn insulation is particularly vulnerable to partial discharge (PD) damage due to high *dV/dt* power converters. This results in uneven voltage distribution and increased voltage drop in the initial winding turns. Environmental factors, like humidity and temperature, impact the partial discharge inception voltage (PDIV), as noted in [1] and [2]. At room temperature (25°C), growing humidity values reduce PDIV, while the opposite occurs at higher temperatures (90°C) [2]. Moreover, high relative humidity (RH) (e.g., 90%) shortens the insulation's lifetime in the presence of PD activity [3]. However, there's a lack of studies explaining the increased PD-induced damage with rising humidity. Therefore, this paper seeks to investigate the impact of humidity on streamer inception parameters (SIPs), including effective ionization coefficient of air (α_{eff}), partial discharge (PD) inception field (E_{inc}), critical field line length (CFLL), and firing voltage (V_{firing}), derived from the Schumann's streamer inception criterion (SCSIC), to explain why PD-induced damage is more pronounced at higher humidity levels.

For the PD-free insulation design purpose, especially with purely organic insulation (Type I) and PD as the end-of-life criterion [4], a PDIV prediction model based on SCSIC represents a valuable tool. Existing SCSIC research, such as [5]-[10], uses a constant humidity level to predict PDIV. Yet, in real applications, humidity can vary, affecting predicted PDIV and insulation system reliability. Therefore, addressing this gap, the paper also aims to examine how humidity affects the fitting parameter K from 25°C to 90°C. The focus is on ionization swarm parameters of air, utilizing FEM simulations while neglecting the impact of humidity on the wire insulation's surface conductivity.

II. METHODOLOGY

The adopted methodology consists of three steps:

- Measuring PDIV for twisted pairs (TPs) at 25°C and 90°C with varying RH.
- Conducting electric field distribution simulations and considering ionization swarm parameters at the B10 PDIV level (10% probability from the 2-parameter Weibull distribution) for diverse RH scenarios.
- Using SCSIC to derive parameter K and SIPs at the 10% probability level corresponding to each RH and temperature pair.

A. Test Samples to Measure PDIV

PDIV measurements are performed on TPs representing random-wound electrical machine insulation systems. Insulated wire specifications are provided in Table I. Details on measuring copper wire diameter, insulation thickness, and relative permittivity can be found in [8] and [9]. The insulation for round magnet wire is grade II, featuring a THEIC-modified polyester-imide base and a polyamide-imide topcoat, both with a 220°C thermal class. TPs are manufactured by twisting wires 12 times with a 7 N load tension [11]. Each test condition (varied RH at 25°C and 90°C) involves a dataset comprising five pristine, non-electrically stressed TPs.

TABLE I
INSULATED WIRE SPECIFICATIONS

Parameter	Value
Bare copper wire diameter	0.556 mm
Insulation thickness	28.5 μm
Relative permittivity	4.31
Insulation grade	Grade II
Insulation basecoat	THEIC-modified polyester-imide
Insulation overcoat	Polyamide-imide
Thermal class	220°C

B. PDIV Test Setup

For evaluating turn-to-turn insulation in inverter-fed motors, IEC 60034-18-41 [4] recommends PDIV measurements with either sinusoidal or impulsive voltage sources. Employing a 50 Hz AC supply provides a cautious assessment of turn-to-turn insulation compared to the 2-level inverter or surge generator waveforms [5]-[10]. Therefore, this study opts for AC PDIV tests using a 50 Hz sinusoidal waveform, ensuring a conservative insulation qualification approach.

Fig. 1 schematizes that the PDIV testing takes place within an ESPEC ARS-0220 environmental chamber having a test volume of 0.22 m³ providing precise temperature and humidity

control. Test leads enter the climate chamber through a rubber plug, safeguarding against external temperature and humidity influences. The AC power source, Megger 4110, generates 50 Hz voltage excitation. The voltage across the TP is measured using a high-voltage differential probe (PICO® TA044) with a 70 MHz bandwidth, 1000:1 voltage attenuation ratio, and 10 MΩ impedance, monitored with a Keysight® DSOX2024A oscilloscope. To detect PD waveform, a custom indirect circuit, with a 4.7 nF coupling capacitor in parallel to the specimen is used to improve sensitivity and signal-to-noise ratio. The PD sensor is a Kanggaote (KGT) HFCT with a bandwidth spanning from 0.3 to 100 MHz, directly connected to the oscilloscope.
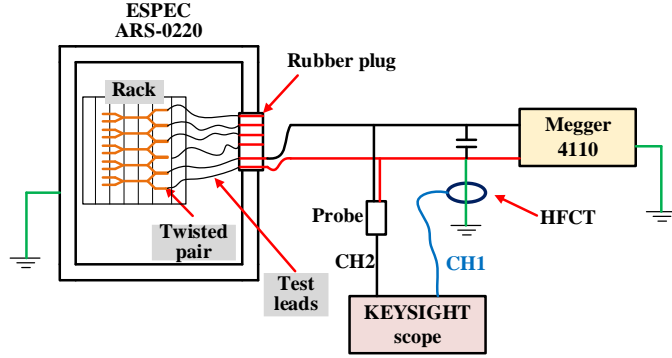
Fig. 1. Schematic depicting the configuration and arrangement of PDIV testing setup and connections.

C. Test Conditions and Measurement Procedure

PDIV tests cover seven RH levels (30%, 40%, 50%, 60%, 70%, 80%, and 90%) at two constant temperatures: 25°C and 90°C, yielding 14 case studies. Before each test, time is allotted for RH and temperature stabilization. Voltage is incrementally raised in 10 V steps, with a 2-minute wait at each step to ensure precise PDIV measurements. Detected PD peak voltages are recorded as PDIV. Data from testing five pristine TPs for each RH and temperature pair is fitted to a 2-parameter Weibull distribution. The B10 value at 90°C is divided by that at 25°C, providing the normalized PDIV at 90°C.

III. DERIVING SIPs THROUGH SCSIC

Considering the SCSIC [12], the transition from Townsend to streamer discharges takes place when condition (1) is met by at least one electric field line (FL) [5]-[10], and [13]:

$$K \leq \int_0^{x_c} \alpha_{\text{eff}}(x) \cdot dx \qquad (1)$$

K, the Schumann constant, is dimensionless. x denotes the electron's travel distance across the FL from cathode to anode, while x_c represents the critical avalanche length beyond which Townsend discharges transition into streamer discharges, initiating the earliest discharge event. In (1), α_{eff} stands for the effective ionization coefficient of air, corresponding to the electric field across the FL as defined in (2):

$$\alpha_{\text{eff}} = \alpha - \eta \qquad (2)$$

where α and η, denoting ionization and attachment coefficients of air, depending on electric field strength, gas number density or its pressure, temperature, and humidity level.

The process of deriving K and SIPs explained in [7]-[10], involves determining K as the maximum value from the right-hand term in (1) under B10 of PDIV. This is done by considering all FLs within the air wedge between two insulated wires, at different humidity levels, and temperatures of 25°C and 90°C. Subsequently, the FL with the highest K is identified as the critical field line (CFL). Parameters associated with CFL are then determined for each tested condition. These parameters include α_{eff}, electric field intensity E_{inc}, CFLL, and V_{firing}.

IV. RESULTS AND DISCUSSIONS
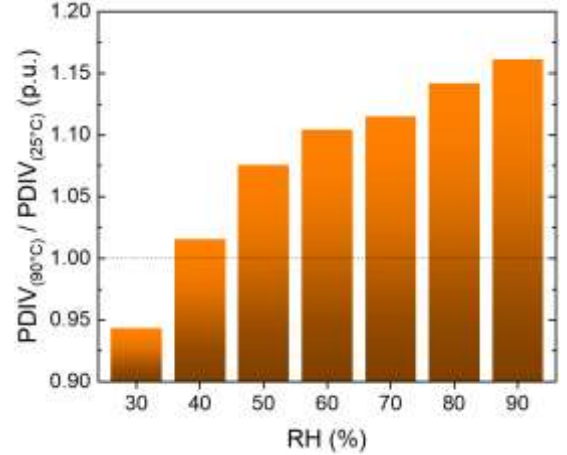
Fig. 2. Variation in B10 of PDIV peak at 90°C as a function of RH, normalized to the measured value at 25°C.

A. Measured PDIV

In Fig. 2, PDIV$_{(90°C)}$ surpasses PDIV$_{(25°C)}$ at RH≥40%, with the difference intensifying as humidity rises to approximately 1.6% at RH=40% and 16.1% at RH=90%. The rising PDIV$_{(90°C)}$ as a function of the humidity can be attributed to three concurrent factors:

- Increased air attachment coefficient (η) with higher humidity due to water's electronegativity as speculated in [1] and demonstrated in [13],
- Enhanced surface conductivity from high temperature and humidity [14], and
- Elevated losses (tanδ) at higher humidity levels [15], [16].

However, at lower RH (e.g., RH=30%), the impact of temperature prevails, leading to a 5.7% smaller PDIV$_{(90°C)}$ compared to PDIV$_{(25°C)}$ due to the reduced air density. Indeed, lower gas number density leads to longer mean free paths for electron-gas molecule collisions, enabling electrons to gain more kinetic energy and initiate ionization events more easily, thus requiring less voltage for PD inception. Notably, the limited value of PDIV$_{(90°C)}$ at RH=30% is not caused by the increment of insulation permittivity, as polyamide-imide's permittivity remains almost stable from 25°C to 90°C [1].

B. Schumann Constant (K)

In Fig. 3, $K_{(90°C)}$ exceeds $K_{(25°C)}$ by 17.3% at RH=30% and 25% at RH=40%, signifying over-conservative predictions when using $K_{(25°C)}$ to estimate PDIV at 90°C. On the other hand, an underestimated prediction is obtained when using $K_{(90°C)}$ to forecast PDIV at 25°C at low RH levels based on SCSIC. Between RH=50% and RH=90%, $K_{(90°C)}$ is smaller than $K_{(25°C)}$,

with the difference decreasing as RH rises. For example, $K_{(90°C)}$ is 38.4% and 20.5% lower than $K_{(25°C)}$ at RH=50% and RH=90% respectively. Therefore, extreme caution is required when employing $K_{(25°C)}$ to forecast PDIV at 90°C within the RH range from 50% to 90%, as it leads to an overestimated PDIV (especially at RH=50%). Conversely, underestimated PDIV predictions are achieved when $K_{(90°C)}$ is used to predict PDIV at 25°C within the same RH range. The sharp decline in $K_{(90°C)}$ between RH=40% and RH=50% is due to a substantial reduction in α_{eff} as the critical region (CritR) of α_{eff} disappears at 90°C in this RH range (see Fig. 4b).
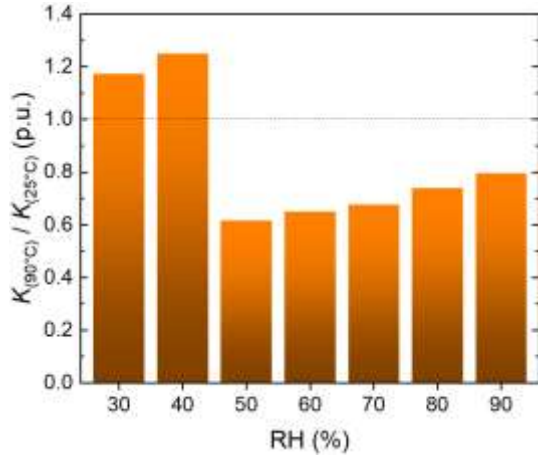
Fig. 3. Variation in K at 90°C as a function of RH, normalized to the derived value at 25°C.

C. Critical Region (CritR) of α_{eff}

In Fig. 4a, α_{eff} at 25°C is almost consistent across all field line lengths (FLLs) regardless of RH levels. In contrast, Fig. 4b reveals that at 90°C and RH from 30% to 40%, the CritR becomes smaller, less dense, and shifts toward higher electric fields and shorter FLLs compared to 25°C (Fig. 4a). Notably, the CritR vanishes from RH=40% to RH=50% at 90°C, resulting in a significant reduction in α_{eff} across the CFL, (Fig. 5), where maximum K is achieved under PDIV. This CritR disappearance leads to abrupt changes in SIPs, such as K (Fig. 3), α_{eff}, and E_{inc} (Fig. 5), and CFLL and V_{firing} (Fig. 6). Furthermore, Fig. 4b indicates that at 90°C, α_{eff} remains stable at high electric fields (i.e., short FLLs), but increases at low electric fields (long FLLs), suggesting that the impact of increasing η at higher RH levels, as speculated in [1], is less prominent at elevated temperatures (i.e., 90°C), while the vanishing of the CritR plays a more crucial role in these SIP variations.

D. α_{eff} and E_{inc}

In Fig. 5, at 90°C, α_{eff} exceeds that at 25°C for RH≤40% (by approximately 44.6%), but significantly reverses for RH≥50% (by approximately 72.4%), reflecting the disappearance of the CritR at 90°C (Fig. 4b). Notably, the α_{eff} ratio at 90°C to 25°C remains relatively stable for both RH ranges (≤40% and 50%≤RH≤80%). The lowest α_{eff} at 90°C compared to 25°C occurs at RH=90% (approximately 76.5%), due to higher η. Fig. 5 illustrates that the electric field intensity ratio, $E_{inc(90°C/25°C)}$, follows a similar RH-dependent trend as $\alpha_{eff(90°C/25°C)}$, but contradicts the CFLL$_{(90°C/25°C)}$ trend (Fig. 6).

For RH≤40%, E_{inc} is slightly higher at 90°C than at 25°C (about 10.1%), while the difference is more pronounced for RH≥50% (39.1% on average). The significant increase in CFLL$_{(90°C/25°C)}$ from RH=40% to RH=50% (Fig. 6) leads to a sharp decrease in $E_{inc(90°C/25°C)}$ (about 43.7%), as longer CFLL corresponds to weaker electric fields. Similar to $\alpha_{eff(90°C/25°C)}$, $E_{inc(90°C/25°C)}$ remains relatively stable for RH≤40% and 50%≤RH≤80%, but E_{inc} at 90°C reaches its lowest point compared to that at 25°C at RH=90% (about 46.1%) due to the longest CFLL$_{(90°C/25°C)}$ for this RH (see Fig. 6).

(a)

(b)
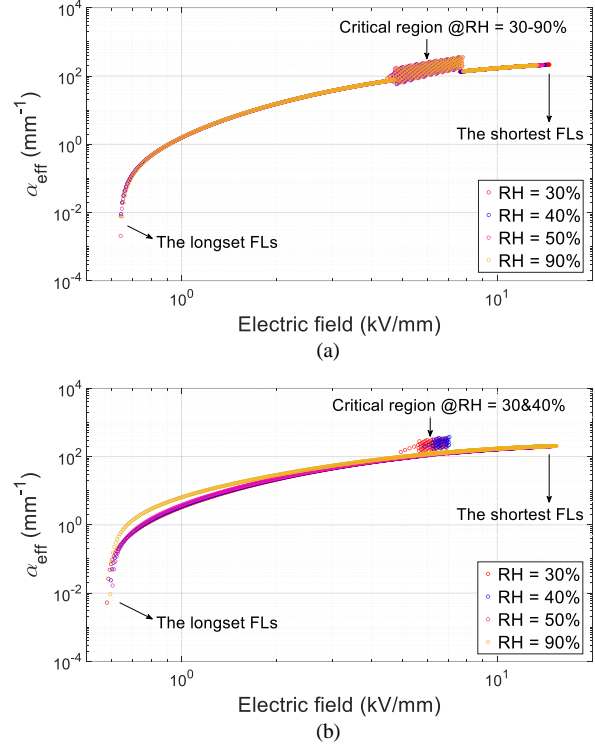
Fig. 4. Humidity impact on α_{eff} at (a) 25°C and (b) 90°C under PDIV corresponding to all the field lines (FLs) ranging from the shortest FLL (E_{max}) to the longest FLL (E_{min}) derived by BOLSIG+.
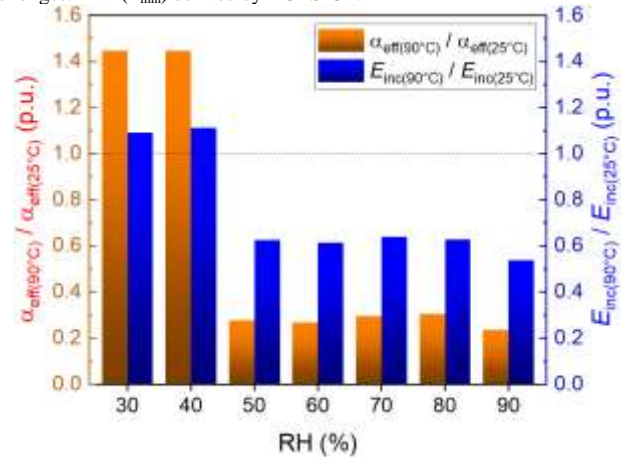
Fig. 5. Variation in α_{eff} and E_{inc} at 90°C as a function of RH, normalized to the derived value at 25°C.

E. CFLL and V_{firing}

In Fig. 6, CFLL at 90°C is shorter than at 25°C for RH≤40% but significantly extends for RH≥50%. For example, at

RH=30%, it's 18.9% shorter, while at RH=90%, it's 238.1% longer. This CFLL increase at 90°C from RH=40% to 50% compensates for reduced α_{eff} due to CritR disappearance (Figs. 4b and 5), ensuring ample ionization for discharges. Indeed, longer CFLLs provide electrons with more kinetic energy, increasing ionization events and enabling critical avalanche sizes for Townsend-to-streamer transitions [8]-[10], and [13]. As $CFLL_{(90°C/25°C)}$ rises with RH, electrons gain more energy at 90°C, causing additional damage in the presence of PD activity and potentially shortening insulation lifetimes at RH=90%, as experimentally confirmed [3]. V_{firing}, obtained from the product of E_{inc} (Fig. 5) and CFLL (Fig. 6), mirrors the $CFLL_{(90°C/25°C)}$ trend in Fig. 6, affirming CFLL's dominant role. For instance, at RH=30%, V_{firing} at 90°C is 11.6% lower, but at RH=90%, it's 82.1% higher than at 25°C. The overall $V_{firing(90°C/25°C)}$ increase with higher RH suggests a corresponding rise in PD charge magnitude at 90°C than 25°C, aligning with the linear relationship between V_{firing} and PD charge [7]. This increase in PD charge amplitude is coupled with the longer CFLL at increased RH, implying more electrons and energy, heightening the risk of insulation degradation through dissociative electron attachment (DEA) in the presence of PD activity, [17], at 90°C and higher RH levels, in particular at RH=90%.
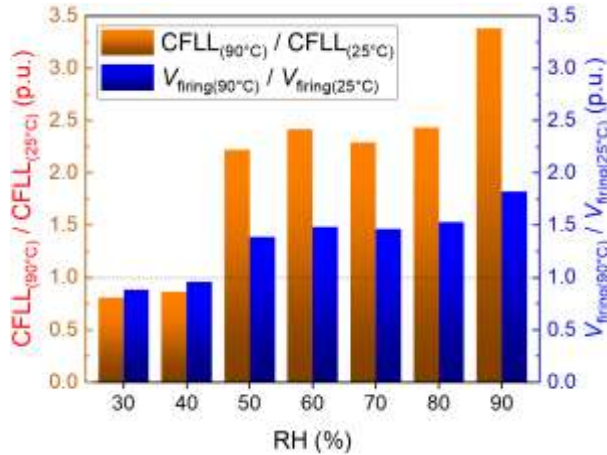
Fig. 6. Variation in CFLL and V_{firing} at 90°C as a function of RH, normalized to the derived value at 25°C.

V. CONCLUSIONS

In conclusion, careful consideration of the RH level is essential when selecting the parameter K for predicting PDIV based on SCSIC. A single K value obtained at 25°C can provide an over-conservative PDIV prediction at 90°C when RH is ≤40%. However, for RH ≥50%, using the derived K value at 25°C to predict PDIV at 90°C is risky as $K_{(25°C)} > K_{(90°C)}$ within this RH range. Additionally, at RH ≥40%, the PDIV at 90°C exceeds that at 25°C, but this doesn't necessarily imply improved insulation performance. The analysis of SCSIC-derived SIPs under high humidity levels clarifies the PD behaviour. These findings reveal increased CFLL and V_{firing} with rising RH, indicating higher discharge energy and PD charge magnitude, as confirmed experimentally with a shorter insulation lifetime at RH=90% in the presence of PD activity. Furthermore, a transition phase is evident at 90°C when RH shifts from 40% to 50%, marked by the disappearance of CritR in α_{eff}. This results in notable variations in key SIPs at 90°C

compared to those of 25°C. Specifically, K, α_{eff}, and E_{inc} decrease significantly, while CFLL and V_{firing} increase, indicating a substantial rise in damage rate during PD activity, when RH is within the range of 40%÷50%.

REFERENCES

[1] Y. Kikuchi *et al.*, "Effects of ambient humidity and temperature on partial discharge characteristics of conventional and nanocomposite enameled magnet wires," *IEEE Trans. Electr. Insul.*, vol. 15, no. 6, pp. 1617-1625, Dec. 2008.

[2] A. Rumi, A. Cavallini and L. Lusuardi, "Combined Effects of Temperature and Humidity on the PDIV of Twisted Pairs," in *2020 IEEE 3rd International Conference on Dielectrics (ICD)*, Valencia, Spain, 2020, pp. 906-909.

[3] P. Wang, Y. Li, A. Cavallini, J. Zhang, E. Xiang, and K. Wang, "The influence of relative humidity on partial discharge and endurance features under short repetitive impulsive voltages," in *2018 IEEE Conference on Electrical Insulation and Dielectric Phenomena (CEIDP)*, Cancun, Mexico, 2018, pp. 506-509.

[4] IEC Std. 60034-18-41, "Rotating electrical machines - part 18-41: partial discharge free electrical insulation systems (Type I) used in rotating electrical machines fed from voltage converters - qualification and quality control tests," 2019.

[5] L. Lusuardi, A. Cavallini, M. G. de la Calle, J. M. Martínez-Tarifa, and G. Robles, "Insulation design of low voltage electrical motors fed by PWM inverters," *IEEE Electr. Insul. Mag.*, vol. 35, no. 3, pp. 7-15, May-Jun. 2019.

[6] J. Gao, A. Rumi, Y. He and A. Cavallini, "Towards a holistic approach to inverter-fed machine design: FEM-based PDIV prediction of complete windings," *IEEE Trans. Electr. Insul.*, pp. 1-9, June 2023.

[7] H. Naderiallaf, M. Degano, and C. Gerada, "PDIV modeling for rectangular wire turn-to-turn insulation of inverter-fed motors through thermal aging," *IEEE Trans. Electr. Insul.*, vol. 31, no. 1, pp. 550-559, Feb. 2024.

[8] H. Naderiallaf, Y. Ji, P. Giangrande, and M. Galea, "Temperature impact on PDIV for turn-to-turn insulation of inverter-fed motors: from ground level to cruising altitude," *IEEE Trans. Electr. Insul.*, pp. 1-10, Sep. 2023.

[9] H. Naderiallaf, Y. Ji, P. Giangrande, and M. Galea, "Air pressure impact on the avalanche size for turn-to-turn insulation of inverter-fed motors," *IEEE Trans. Electr. Insul.*, vol. 31, no. 1, pp. 85-94, Feb. 2024.

[10] H. Naderiallaf, M. Degano, C. Gerada, and D. Gerada "Fillet radius impact of rectangular insulated wires on PDIV for turn-to-turn insulation of inverter-fed motors," *IEEE Trans. Electr. Insul.*, pp. 1-10, Jan. 2024.

[11] *Winding Wires - Test Methods - Part 5: Electrical Properties*, IEC Std. 60851-5, 2008.

[12] W. O. Schumann, "Über das minimum der durchbruchfeldstärke bei kugelelektroden," *Archiv Für Elektrotechnik*, vol. 12, nos. 6–12, pp. 593–608, Jun. 1923.

[13] H. Naderiallaf, Y. Ji, P. Giangrande, and M. Galea, "Modeling humidity impact on PDIV for turn-to-turn insulation of inverter-fed motors at different temperatures," *IEEE Trans. Electr. Insul.*, pp. 1-10, Nov. 2023.

[14] T. Wakimoto, H. Kojima, and N. Hayakawa, "Measurement and evaluation of partial discharge inception voltage for enameled rectangular wires under AC voltage," *IEEE Trans. Electr. Insul.*, vol. 23, no. 6, pp. 3566-3574, Dec. 2016.

[15] Y. Ji *et al.*, "Partial discharge investigation under humidity conditions via dissipation factor and insulation capacitance tip-up test," *IEEE Trans. Electr. Insul.*, vol. 29, no. 4, pp. 1483-1490, Aug. 2022.

[16] H. Naderiallaf, M. Degano, and C. Gerada, "Assessment of edgewise insulated wire bend radius impact on dielectric properties of turn-to-turn insulation through thermal aging," *IEEE Trans. Electr. Insul.*, vol. 31, no. 1, pp. 419-428, Feb. 2024.

[17] H. Naderiallaf, P. Seri and G. C. Montanari, "Effect of voltage slew rate on partial discharge phenomenology during voltage transient in HVDC insulation: the case of polymeric cables," *IEEE Trans. Electr. Insul.*, vol. 29, no. 1, pp. 215-222, Feb. 2022.